CDM in Supersymmetric Models

Keith A. Olive[a]

[a] *Theoretical Physics Institute, School of Physics and Astronomy*
University of Minnesota, Minneapolis, MN 55455

Abstract

The supersymmetric extension to the Standard Model offers a promising cold dark matter candidate, the lightest neutralino. I will review the phenomenological and cosmological constraints on the supersymmetric parameter space and discuss the prospects for the detection of this candidate in both accelerator and direct detection searches.

1 Introduction

It is well known that supersymmetric models with conserved R-parity contain one new stable particle which is a candidate for cold dark matter (CDM) [1]. There are very strong constraints, however, forbidding the existence of stable or long lived particles which are not color and electrically neutral. Strong and electromagnetically interacting LSPs would become bound with normal matter forming anomalously heavy isotopes. Indeed, there are very strong upper limits on the abundances, relative to hydrogen, of nuclear isotopes [2], $n/n_H \lesssim 10^{-15}$ to 10^{-29} for 1 GeV $\lesssim m \lesssim$ 1 TeV. A strongly interacting stable relic is expected to have an abundance $n/n_H \lesssim 10^{-10}$ with a higher abundance for charged particles. There are relatively few supersymmetric candidates which are not colored and are electrically neutral. The sneutrino [3, 4] is one possibility, but in the MSSM, it has been excluded as a dark matter candidate by direct [5] and indirect [6] searches. In fact, one can set an accelerator based limit on the sneutrino mass from neutrino counting, $m_{\tilde{\nu}} \gtrsim 44.7$ GeV [7]. In this case, the direct relic searches in underground low-background experiments require $m_{\tilde{\nu}} \gtrsim 20$ TeV [5]. Another possibility is the gravitino which is probably the most difficult to exclude. I will concentrate on the remaining possibility in the MSSM, namely the neutralinos.

There are four neutralinos, each of which is a linear combination of the $R = -1$, neutral fermions [1]: the wino $\tilde{W}^3$, the partner of the 3rd component of the $SU(2)_L$ gauge boson; the bino, $\tilde{B}$, the partner of the $U(1)_Y$ gauge boson; and the two neutral Higgsinos, $\tilde{H}_1$ and $\tilde{H}_2$. In general, neutralinos can be expressed as a linear combination

$$\chi = \alpha\tilde{B} + \beta\tilde{W}^3 + \gamma\tilde{H}_1 + \delta\tilde{H}_2 \tag{1}$$

The solution for the coefficients α, β, γ and δ for neutralinos that make up the LSP can be found by diagonalizing the mass matrix

$$(\tilde{W}^3, \tilde{B}, \tilde{H}_1^0, \tilde{H}_2^0) \begin{pmatrix} M_2 & 0 & \frac{-g_2 v_1}{\sqrt{2}} & \frac{g_2 v_2}{\sqrt{2}} \\ 0 & M_1 & \frac{g_1 v_1}{\sqrt{2}} & \frac{-g_1 v_2}{\sqrt{2}} \\ \frac{-g_2 v_1}{\sqrt{2}} & \frac{g_1 v_1}{\sqrt{2}} & 0 & -\mu \\ \frac{g_2 v_2}{\sqrt{2}} & \frac{-g_1 v_2}{\sqrt{2}} & -\mu & 0 \end{pmatrix} \begin{pmatrix} \tilde{W}^3 \\ \tilde{B} \\ \tilde{H}_1^0 \\ \tilde{H}_2^0 \end{pmatrix} \tag{2}$$

where $M_1(M_2)$ are the soft supersymmetry breaking U(1) (SU(2)) gaugino mass terms. μ is the supersymmetric Higgs mixing mass parameter and since there are two Higgs doublets in the MSSM, there are two vacuum expectation values, v_1 and v_2. One combination of these is related to the Z mass, and therefore is not a free parameter, while the other combination, the ratio of the two vevs, $\tan\beta$, is free.

The most general version of the MSSM, despite its minimality in particles and interactions contains well over a hundred new parameters. The study of such a model would be untenable were it not for some (well motivated) assumptions. These have to do with the parameters associated with supersymmetry breaking. It is often assumed that, at some unification scale, all of the gaugino masses receive a common mass, $m_{1/2}$. The gaugino masses at the weak scale are determined by running a set of renormalization group equations. Similarly, one often assumes that all scalars receive a common mass, m_0, at the GUT scale (though one may wish to make an exception for the Higgs soft masses). These

too are run down to the weak scale. The remaining supersymmetry breaking parameters are the trilinear mass terms, A_0, which I will also assume are unified at the GUT scale, and the bilinear mass term B. There are, in addition, two physical CP violating phases which will not be considered here.

The natural boundary conditions at the GUT scale for the MSSM would include μ, the two soft Higgs masses (m_1 and m_2) and B in addition to $m_{1/2}$, m_0, and A_0. In this case, by running the RGEs down to a low energy scale, one would predict the values of M_Z, $\tan\beta$, and the Higgs pseudoscalar mass, m_A (in addition to all of the sparticle masses). Since M_Z is known, it is more useful to analyze supersymmetric models where M_Z is input rather than output. It is also common to treat $\tan\beta$ as an input parameter. This can be done at the expense of shifting μ (up to a sign) and B from inputs to outputs. When the supersymmetry breaking Higgs soft masses are also unified at the GUT scale (and take the common value m_0), the model is often referred to as the constrained MSSM or CMSSM. Once these parameters are set, the entire spectrum of sparticle masses at the weak scale can be calculated.

2 The Relic Density

The relic abundance of LSP's is determined by solving the Boltzmann equation for the LSP number density in an expanding Universe. The technique [8] used is similar to that for computing the relic abundance of massive neutrinos [9]. The relic density depends on additional parameters in the MSSM beyond $m_{1/2}, \mu$, and $\tan\beta$. These include the sfermion masses, $m_{\tilde{f}}$, as well as m_A, all derived from m_0, A_0, and $m_{1/2}$. To determine the relic density it is necessary to obtain the general annihilation cross-section for neutralinos. In much of the parameter space of interest, the LSP is a bino and the annihilation proceeds mainly through sfermion exchange. Because of the p-wave suppression associated with Majorana fermions, the s-wave part of the annihilation cross-section is suppressed by the outgoing fermion masses. This means that it is necessary to expand the cross-section to include p-wave corrections which can be expressed as a term proportional to the temperature if neutralinos are in equilibrium. Unless the neutralino mass happens to lie near near a pole, such as $m_\chi \simeq m_Z/2$ or $m_h/2$, in which case there are large contributions to the annihilation through direct s-channel resonance exchange, the dominant contribution to the $\tilde{B}\tilde{B}$ annihilation cross section comes from crossed t-channel sfermion exchange.

Annihilations in the early Universe continue until the annihilation rate $\Gamma \simeq \sigma v n_\chi$ drops below the expansion rate given by the Hubble parameter, H. For particles which annihilate through approximate weak scale interactions, this occurs when $T \sim m_\chi/20$. Subsequently, the relic density of neutralinos is fixed relative to the number of relativistic particles. As noted above, the number density of neutralinos is tracked by a Boltzmann-like equation,

$$\frac{dn}{dt} = -3\frac{\dot{R}}{R}n - \langle\sigma v\rangle(n^2 - n_0^2) \tag{3}$$

where n_0 is the equilibrium number density of neutralinos. By defining the quantity

$f = n/T^3$, we can rewrite this equation in terms of $x = T/m_\chi$, as

$$\frac{df}{dx} = m_\chi \left(\frac{4}{45}\pi^3 G_N N\right)^{-1/2} \langle\sigma v\rangle (f^2 - f_0^2) \tag{4}$$

where N is the number of relativistic degrees of freedom. The solution to this equation at late times (small x) yields a constant value of f, so that $n \propto T^3$. The final relic density expressed as a fraction of the critical energy density can be written as [1]

$$\Omega_\chi h^2 \simeq 1.9 \times 10^{-11} \left(\frac{T_\chi}{T_\gamma}\right)^3 N_f^{1/2} \left(\frac{\mathrm{GeV}}{a x_f + \frac{1}{2} b x_f^2}\right) \tag{5}$$

where $(T_\chi/T_\gamma)^3$ accounts for the subsequent reheating of the photon temperature with respect to χ, due to the annihilations of particles with mass $m < x_f m_\chi$ [10]. The subscript f refers to values at freeze-out, i.e., when annihilations cease. The coefficients a and b are related to the partial wave expansion of the cross-section, $\sigma v = a + bx + \ldots$. Eq. (5) results in a very good approximation to the relic density expect near s-channel annihilation poles, thresholds and in regions where the LSP is nearly degenerate with the next lightest supersymmetric particle [11].

The preferred range of the relic LSP density is provided by data on the cosmic microwave background (CMB), which have recently been used to obtain the following 95% confidence range: $\Omega_{\mathrm{CDM}} h^2 = 0.12 \pm 0.04$ [12]. Values much smaller than $\Omega_{\mathrm{CDM}} h^2 = 0.10$ seem to be disfavoured by earlier analyses of structure formation in the CDM framework, so we restrict our attention to $\Omega_{\mathrm{CDM}} h^2 > 0.1$. However, one should note that the LSP may not constitute all the CDM, in which case Ω_{LSP} could be reduced below this value. On the upper side, it is preferable to remain very conservative, in particular because the upper limit on Ω_{LSP} sets the upper limit for the sparticle mass scale. Here, $\Omega_{\mathrm{CDM}} h^2 < 0.3$ is used, while being aware that the lower part of this range currently appears the most plausible.

Fig. 1 illustrates qualitatively the regions of the $(m_{1/2}, m_0)$ plane favoured by LEP limits, particularly on m_h, $b \to s\gamma$ and cosmology. Electroweak symmetry breaking is not possible in the dark-shaded triangular region in the top left corner, and the lightest supersymmetric particle would be charged in the bottom right dark-shaded triangular region. The experimental constraints on m_h and $b \to s\gamma$ exert pressures from the left, as indicated, which depend on the value of $\tan\beta$ and the sign of μ. The indication of a deviation from the Standard Model in $g_\mu - 2$ disfavours $\mu < 0$ and large values of m_0 and $m_{1/2}$ for $\mu > 0$. The region where $\Omega_\chi h^2$ falls within the preferred range is indicated in light shading, its exact shape being dependent on the value of $\tan\beta$. As discussed later in more detail, in addition to the 'bulk' region at low m_0 and $m_{1/2}$, there are a number of regions at large values of $m_{1/2}$ and/or m_0 where the relic density is still compatible with the cosmological constraints. At large values of $m_{1/2}$, the lighter stau, becomes nearly degenerate with the neutralino and coannihilations between these particles must be taken into account [13, 14]. For non-zero values of A_0, there are new regions for which $\chi - \tilde{t}$ coannihilations are important [15]. At large $\tan\beta$, as one increases $m_{1/2}$, the pseudoscalar mass, m_A begins to drop so that there is a wide funnel-like region (at all values of m_0) such that $2m_\chi \approx m_A$ and s-channel annihilations become important [16, 17]. Finally,

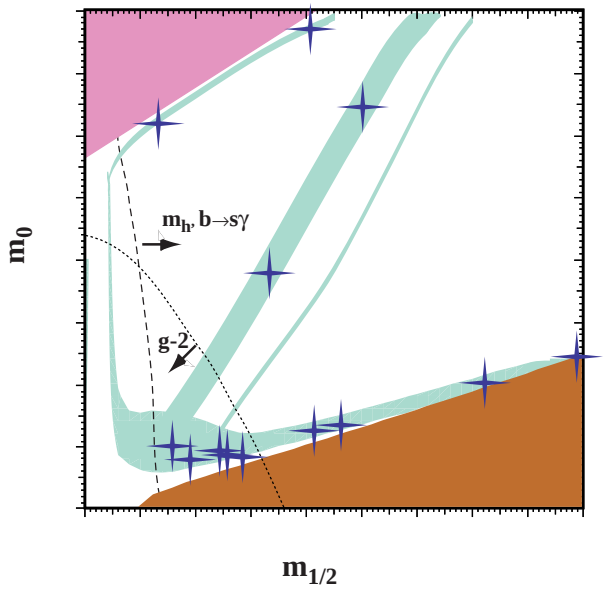

Figure 1: *Qualitative overview of a generic* $(m_{1/2}, m_0)$ *plane. The light (turquoise) shaded area is the cosmologically preferred region with* $0.1 \leq \Omega_\chi h^2 \leq 0.3$. *In the dark (brick red) shaded region at bottom right, the LSP is the charged* $\tilde{\tau}_1$, *so this region is excluded. Electroweak symmetry breaking is not possible in the dark (pink) shaded region at top left. The LEP experimental constraints, in particular that on* m_h, *and measurements of* $b \to s\gamma$ *exert pressure from the left side. The BNL E821 measurement of* $g_\mu - 2$ *favours relatively low values of* m_0 *and* $m_{1/2}$ *for* $\mu > 0$.

there is a region at very high m_0 where the value of μ begins to fall and the LSP becomes more Higgsino-like. This is known as the 'focus point' region [18]. Also shown are the position of several benchmark points chosen for detailed phenomenological study [19].

Let us first focus on the 'bulk' region in the CMSSM for $\tan\beta = 10$ and $\mu > 0$ shown in Fig. 2 [13]. The light shaded region correspond to $0.1 < \Omega_\chi h^2 < 0.3$. The dark shaded region has $m_{\tilde{\tau}_1} < m_\chi$ and is excluded. The light dashed contours indicate the corresponding region in $\Omega_\chi h^2$ if one ignores the effect of coannihilations. Neglecting coannihilations, one would find an upper bound of $\sim 450\,\mathrm{GeV}$ on $m_{1/2}$, corresponding to an upper bound of roughly $200\,\mathrm{GeV}$ on $m_{\tilde{B}}$.

Coannihilations are important when there are several particle species i, with different masses, and each with its own number density n_i and equilibrium number density $n_{0,i}$. In this case [11], the rate equation (3) still applies, provided n is interpreted as the total number density,

$$n \equiv \sum_i n_i \ , \tag{6}$$

n_0 as the total equilibrium number density,

$$n_0 \equiv \sum_i n_{0,i} \ , \tag{7}$$

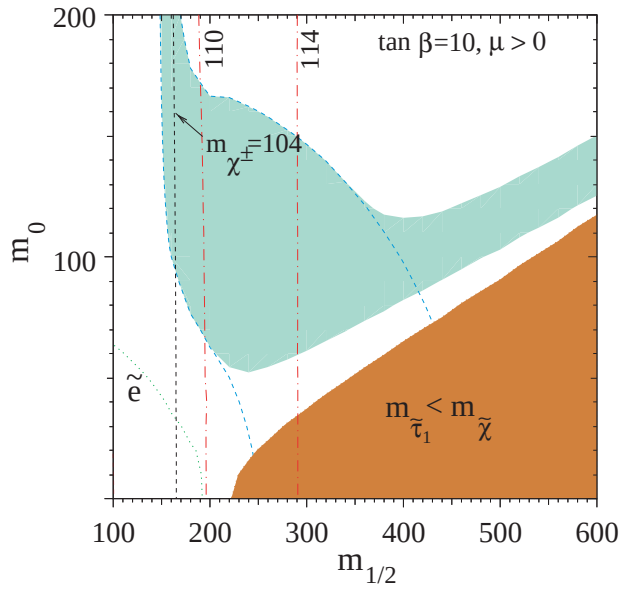

Figure 2: *The light-shaded 'bulk' area is the cosmologically preferred region with* $0.1 \leq \Omega_\chi h^2 \leq 0.3$. *The light dashed lines show the location of the cosmologically preferred region if one ignores coannihilations with the light sleptons. In the dark shaded region in the bottom right, the LSP is the* $\tilde{\tau}_1$*, leading to an unacceptable abundance of charged dark matter. Also shown is the isomass contour* $m_{\chi^\pm} = 104$ *GeV and* $m_h = 110, 114$ *GeV, as well as an indication of the slepton bound from LEP.*

and the effective annihilation cross section as

$$\langle \sigma_{\rm eff} v_{\rm rel} \rangle \equiv \sum_{ij} \frac{n_{0,i} n_{0,j}}{n_0^2} \langle \sigma_{ij} v_{\rm rel} \rangle \ . \tag{8}$$

In eq. (4), m_χ is now understood as the mass of the lightest sparticle under consideration.

Note that this implies that the ratio of relic densities computed with and without coannihilations is, roughly,

$$R \equiv \frac{\Omega^0}{\Omega} \approx \left(\frac{\hat{\sigma}_{\rm eff}}{\hat{\sigma}_0} \right) \left(\frac{x_f}{x_f^0} \right), \tag{9}$$

where $\hat{\sigma} \equiv a + bx/2$ and sub- and superscripts 0 denote quantities computed ignoring coannihilations. The ratio $x_f^0/x_f \approx 1 + x_f^0 \ln(g_{\rm eff}\sigma_{\rm eff}/g_1\sigma_0)$, where $g_{\rm eff} \equiv \sum_i g_i (m_i/m_1)^{3/2} e^{-(m_i - m_1)/T}$. For the case of three degenerate slepton NLSPs, $g_{\rm eff} = \sum_i g_i = 8$ and $x_f^0/x_f \approx 1.2$.

The effect of coannihilations is to create an allowed band about 25-50 GeV wide in m_0 for $m_{1/2} \lesssim 1400\,{\rm GeV}$, which tracks above the $m_{\tilde{\tau}_1} = m_\chi$ contour. Along the line $m_{\tilde{\tau}_1} = m_\chi$, $R \approx 10$, from (9) [13]. As m_0 increases, the mass difference increases and the slepton contribution to $\hat{\sigma}_{\rm eff}$ falls, and the relic density rises abruptly.

3 The CMSSM with Universal Higgs masses

A larger view of the $\tan\beta = 10$ parameter plane is shown in Fig. 3 [21, 17, 19, 22, 23]. Included here are the most important phenomenological constraints (shown schematically

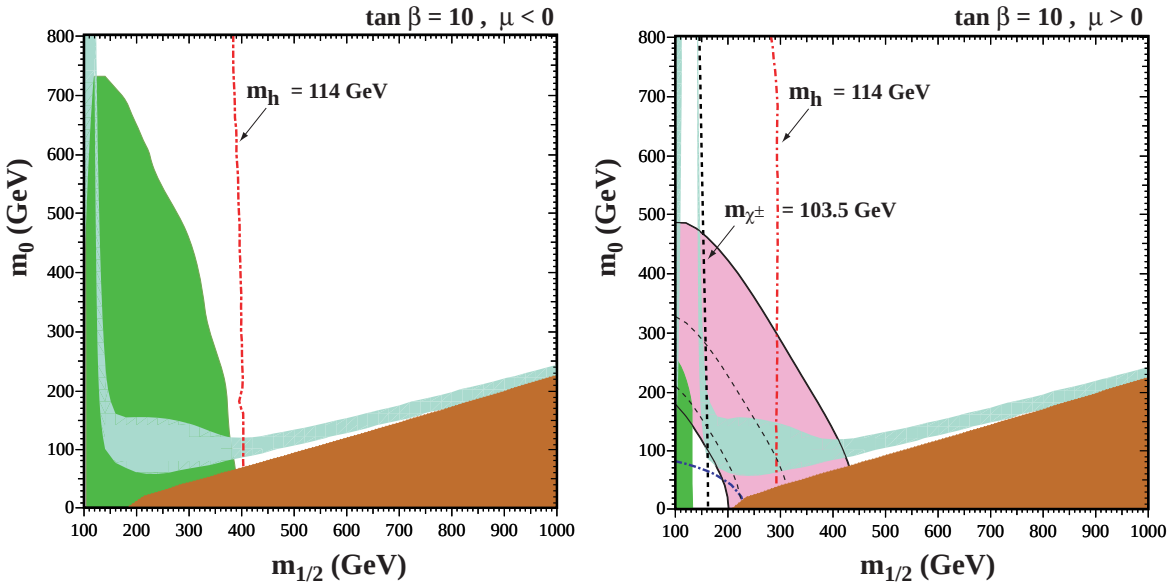

Figure 3: *The $(m_{1/2}, m_0)$ planes for (a) $\tan\beta = 10$ and $\mu < 0$, (b) $\tan\beta = 10$ and $\mu > 0$, assuming $A_0 = 0, m_t = 175$ GeV and $m_b(m_b)^{\overline{MS}}_{SM} = 4.25$ GeV. The near-vertical (red) dot-dashed lines are the contours $m_h = 114$ GeV as calculated using* `FeynHiggs` *[20], and the near-vertical (black) dashed line is the contour $m_{\chi^\pm} = 103.5$ GeV, shown only in (b). Also shown in (b) by the dot-dashed curve in the lower left is the corner excluded by the LEP bound of $m_{\tilde{e}} > 99$ GeV. The medium (dark green) shaded region is excluded by $b \to s\gamma$, and the light (turquoise) shaded area is the cosmologically preferred regions with $0.1 \leq \Omega_\chi h^2 \leq 0.3$. In the dark (brick red) shaded region, the LSP is the charged $\tilde{\tau}_1$. The region allowed by the E821 measurement of a_μ at the 2-σ level, is shaded (pink) and bounded by solid black lines, with dashed lines indicating the 1-σ ranges.*

in Figure 1). These include the constraints on the MSSM parameter space that are provided by direct sparticle searches at LEP, including that on the lightest chargino $\chi^\pm$: $m_{\chi^\pm} \gtrsim 103.5$ GeV [24], and that on the selectron $\tilde{e}$: $m_{\tilde{e}} \gtrsim 99$ GeV [25]. Another important constraint is provided by the LEP lower limit on the Higgs mass: $m_H > 114.4$ GeV [26] in the Standard Model. Since m_h is sensitive to sparticle masses, particularly $m_{\tilde{t}}$, via loop corrections, the Higgs limit also imposes important constraints on the CMSSM parameters, principally $m_{1/2}$.

The constraint imposed by measurements of $b \to s\gamma$ [27] also excludes small values of $m_{1/2}$. These measurements agree with the Standard Model, and therefore provide bounds on MSSM particles, such as the chargino and charged Higgs masses, in particular. Typically, the $b \to s\gamma$ constraint is more important for $\mu < 0$, but it is also relevant for $\mu > 0$, particularly when $\tan\beta$ is large.

The latest value of the anomalous magnetic moment of the muon reported [28] by the BNL E821 experiment is also taken into account. The world average of $a_\mu \equiv \frac{1}{2}(g_\mu - 2)$ now deviates by $(33.9 \pm 11.2) \times 10^{-10}$ from the Standard Model calculation of [29] using e^+e^- data, and by $(17 \pm 11) \times 10^{-10}$ from the Standard Model calculation of [29] based on τ decay data. Other recent analyses of the e^+e^- data yield similar results. On some of

the subsequent plots, the formal 2-σ range $11.5 \times 10^{-10} < \delta a_\mu < 56.3 \times 10^{-10}$ is displayed. As one can see, the region preferred by $g-2$ overlaps very nicely with the 'bulk' region for $\tan\beta = 10$ and $\mu > 0$.

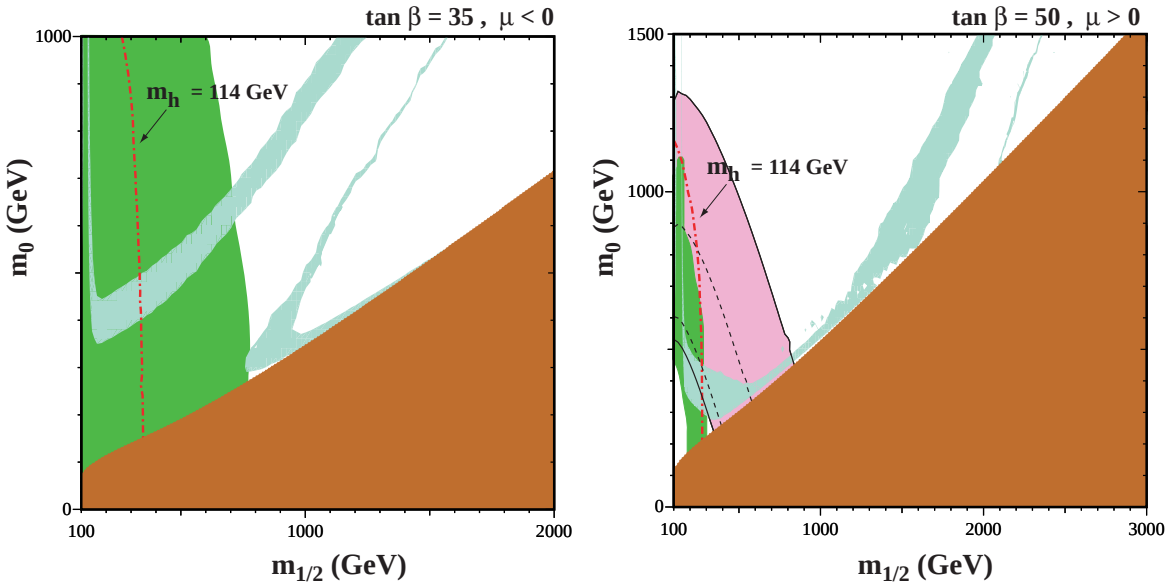

Figure 4: *As in Fig. 3 for (a)* $\tan\beta = 35$ *and* $\mu < 0$ *and (b)* $\tan\beta = 50$ *and* $\mu > 0$

As noted above, another mechanism for extending the allowed CMSSM region to large m_χ is rapid annihilation via a direct-channel pole when $m_\chi \sim \frac{1}{2} m_A$ [16, 17]. Since the heavy scalar and pseudoscalar Higgs masses decrease as $\tan\beta$ increases, eventually $2m_\chi \simeq m_A$ yielding a 'funnel' extending to large $m_{1/2}$ and m_0 at large $\tan\beta$, as seen in Fig. 4. The difficulty and necessary care involved in calculations at large $\tan\beta$ were discussed in [17]. For related CMSSM calculations see [30].

Another way to see the effects of increasing $\tan\beta$ is plot look at the $\tan\beta - m_{1/2}$ plane for fixed m_0. This is shown in Fig. 5. As one can see, there is a charged $\tilde{\tau}_1$ LSP in the upper right corner for both values of m_0, though the area is reduced when m_0 is increased as is expected. One also sees the cosmological region moving up in $\tan\beta$ as m_0 is increased. In b), one also sees the well defined coannihilation tail. Here, the importance of $b \to s\gamma$ at large $\tan\beta$ is clearly displayed.

4 The CMSSM with Non-Universal Higgs masses

If one relaxes the unification condition for the two soft Higgs mass, m_1 and m_2, one could decide to make μ and m_A inputs and instead making the Higgs soft masses outputs. This is referred to as the CMSSM with non-universal Higgs masses or NUHM [31, 32, 23]. The attractive feature of radiative symmetry breaking in the CMSSM is maintained by using the electroweak minimization conditions to solve for m_1 and m_2, given values of μ and m_A at the weak scale.

The electroweak symmetry breaking conditions may be written in the form:

$$m_A^2(Q) = m_1^2(Q) + m_2^2(Q) + 2\mu^2(Q) + \Delta_A(Q) \tag{10}$$

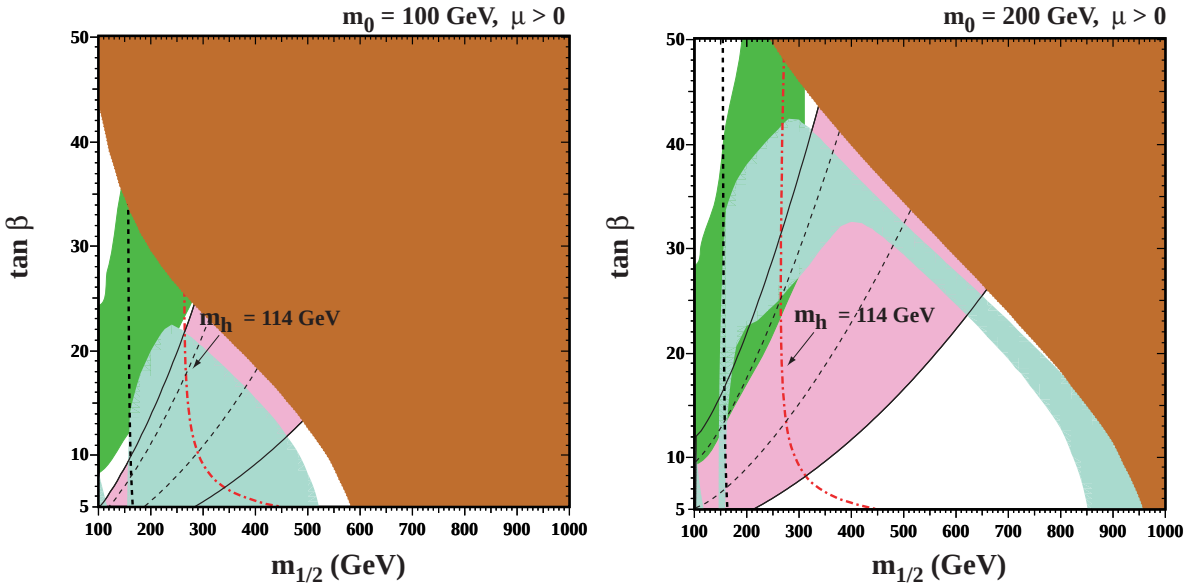

Figure 5: *The* $\tan\beta$ *-* $m_{1/2}$ *plane for (a)* $m_0 = 100$ *GeV and (b)* $m_0 = 200$ *GeV both for* $\mu > 0$*. All shading and line types are as in the previous figures.*

and

$$\mu^2 = \frac{m_1^2 - m_2^2\tan^2\beta + \frac{1}{2}m_z^2(1-\tan^2\beta) + \Delta_\mu^{(1)}}{\tan^2\beta - 1 + \Delta_\mu^{(2)}}, \tag{11}$$

where Δ_A and $\Delta_\mu^{(1,2)}$ are loop corrections [33, 34, 35] and $m_{1,2} \equiv m_{1,2}(m_z)$. The known radiative corrections [33, 36, 37] c_1, c_2 and c_μ relating the values of the NUHM parameters at Q to their values at m_z are incorporated:

$$\begin{aligned} m_1^2(Q) &= m_1^2 + c_1 \\ m_2^2(Q) &= m_2^2 + c_2 \\ \mu^2(Q) &= \mu^2 + c_\mu\,. \end{aligned} \tag{12}$$

Solving for m_1^2 and m_2^2, one has

$$\begin{aligned} m_1^2(1+\tan^2\beta) &= m_A^2(Q)\tan^2\beta - \mu^2(\tan^2\beta + 1 - \Delta_\mu^{(2)}) - (c_1 + c_2 + 2c_\mu)\tan^2\beta \\ &\quad -\Delta_A(Q)\tan^2\beta - \frac{1}{2}m_z^2(1-\tan^2\beta) - \Delta_\mu^{(1)} \end{aligned} \tag{13}$$

and

$$\begin{aligned} m_2^2(1+\tan^2\beta) &= m_A^2(Q) - \mu^2(\tan^2\beta + 1 + \Delta_\mu^{(2)}) - (c_1 + c_2 + 2c_\mu) \\ &\quad -\Delta_A(Q) + \frac{1}{2}m_z^2(1-\tan^2\beta) + \Delta_\mu^{(1)}, \end{aligned} \tag{14}$$

which are used to perform the numerical calculations [23].

It can be seen from (13) and (14) that, if m_A is too small or μ is too large, then m_1^2 and/or m_2^2 can become negative and large. This could lead to $m_1^2(M_X) + \mu^2(M_X) < 0$ and/or $m_2^2(M_X) + \mu^2(M_X) < 0$, thus triggering electroweak symmetry breaking at the GUT scale. The requirement that electroweak symmetry breaking occurs far below the GUT scale forces one to impose the conditions $m_1^2(M_X) + \mu(M_X), m_2^2(M_X) + \mu(M_X) > 0$ as extra constraints, which we call the GUT stability constraint [1].

The NUHM parameter space was recently analyzed [23] and a sample of the results found is shown in Fig. 6. While much of the cosmologically preferred area with $\mu < 0$ is excluded, there is a significant enhancement in the allowed parameter space for $\mu > 0$.

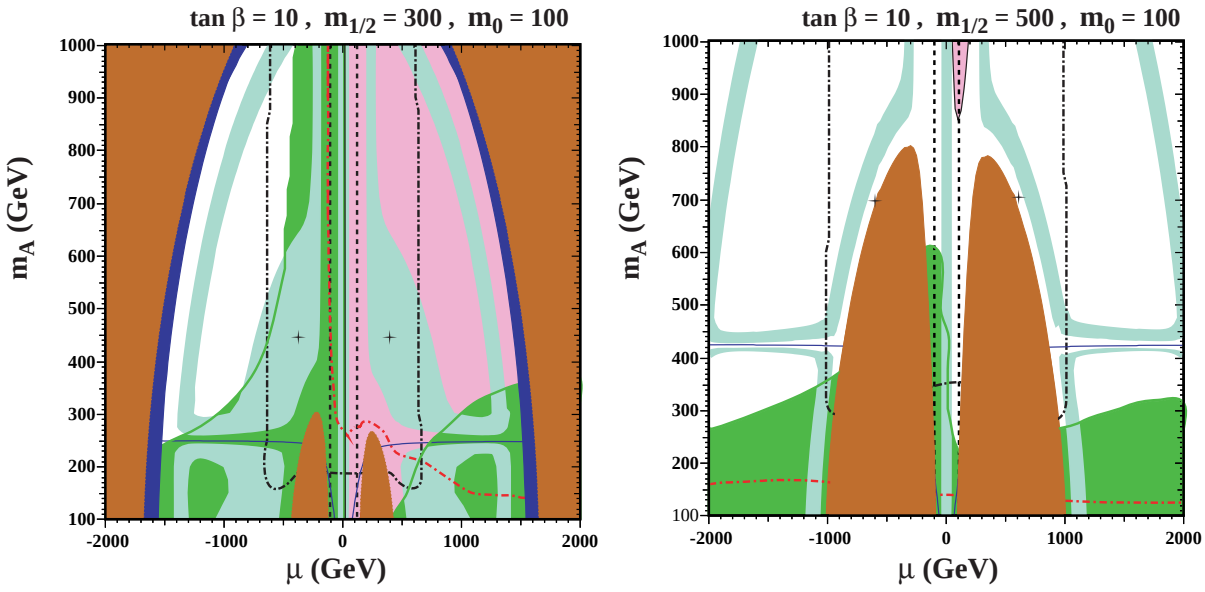

Figure 6: *The NUHM (μ, m_A) planes for* $\tan\beta = 10$, *(a)* $m_0 = 100$ *GeV and* $m_{1/2} = 300$ *GeV and (b)* $m_0 = 100$ *GeV and* $m_{1/2} = 500$ *GeV, with* $A_0 = 0$. *The (red) dot-dashed lines are the contours* $m_h = 114$ *GeV, and the near-vertical (black) dashed lines are the contours* $m_{\chi^\pm} = 103.5$ *GeV. The dark (black) dot-dashed lines indicate the GUT stability constraint. Only the areas inside these curves (small* μ*) are allowed by this constraint. The light (turquoise) shaded areas are the cosmologically preferred regions with* $0.1 \leq \Omega_\chi h^2 \leq 0.3$. *The dark (brick red) shaded regions is excluded because a charged particle is lighter than the neutralino, and the darker (dark blue) shaded regions is excluded because the LSP is a sneutrino. The medium (green) shaded region is excluded by* $b \to s\gamma$. *The regions allowed by the E821 measurement of* a_μ *at the 2-*σ *level are shaded (pink) and bounded by solid black lines. The solid (blue) curves correspond to* $m_\chi = m_A/2$.

As usual, there are dark (red) regions where there is one or more charged sparticle lighter than the neutralino χ so that χ is no longer the LSP. First, there are 'shark's teeth' at $|\mu| \sim 300$ GeV, $m_A \lesssim 300$ GeV in panel (a) of Fig. 6 where the $\tilde{\tau}_1$ is the LSP. At small $|\mu|$, particularly at small m_A when the mass difference $m_2^2 - m_1^2$ is small, the $\tilde{\tau}_R$ mass is driven small, making the $\tilde{\tau}_1$ the LSP. At even smaller $|\mu|$, however, the lightest neutralino gets lighter again, since $m_\chi \simeq \mu$ when $\mu < M_1 \simeq 0.4\, m_{1/2}$. In addition, there

[1] For a different point of view, however, see [38].

are extended dark (red) shaded regions at large $|\mu|$ where left-handed sleptons become lighter than the neutralino. However, the electron sneutrino $\tilde{\nu}_e$ and the muon sneutrino $\tilde{\nu}_\mu$ (which are degenerate within the approximations used here) have become joint LSPs at a slightly smaller $|\mu|$. Since the possibility of sneutrino dark matter has been essentially excluded by a combination of 'ν counting' at LEP, which excludes $m_{\tilde{\nu}} < 44.7$ GeV [7], and searches for cold dark matter, which exclude heavier $\tilde{\nu}$ weighing $\lesssim 1$ TeV [4], we still demand that the LSP be a neutralino χ. The darker (dark blue) shaded regions are where the sneutrinos are the LSPs, and therefore excluded. In the strips adjacent to the $\tilde{\nu}_{e,\mu}$ LSP regions, neutralino-sneutrino coannihilation is important in suppressing the relic density to an acceptable level [23].

The thick cosmological region at smaller μ corresponds to the 'bulk' region familiar from CMSSM studies. The two (black) crosses indicate the position of the CMSSM points for these input parameters. Extending upward in m_A from this region, there is another light (turquoise) shaded band at smaller $|\mu|$. Here, the neutralino gets more Higgsino-like and the annihilation to W^+W^- becomes important, yielding a relic density in the allowed range [2]. For smaller $|\mu|$, the relic density becomes too small due to the $\chi - \chi' - \chi^+$ coannihilations. For even smaller $|\mu|$ ($\lesssim 30$ GeV) many channels are kinematically unavailable and we are no longer near the h and Z pole. As a result the relic density may again come into the cosmologically preferred region. However, this region is excluded by the LEP limit on the chargino mass.

The unshaded regions between the allowed bands have a relic density that is too high: $\Omega_\chi h^2 > 0.3$. However, the $\tilde{\tau}$ and $\tilde{\nu}$ coannihilation and bulk bands are connected by horizontal bands of acceptable relic density that are themselves separated by unshaded regions of low relic density, threaded by solid (blue) lines asymptoting to $m_A \sim 250$ GeV. These lines correspond to cases when $m_\chi \simeq m_A/2$, where direct-channel annihilation: $\chi + \chi \to A, H$ is important, and suppresses the relic density [17, 16] creating 'funnel'-like regions.

In panel (b), a larger value of $m_{1/2}$ is chosen. In this case, the previous region excluded by the neutral LSP constraint at large $|\mu|$, migrates to larger $|\mu|$. The 'shark's teeth' for moderate $|\mu|$ grow, reaching up to $m_A \sim 800$ GeV. These arise when one combines a large value of $m_{1/2}$ with a relatively small value of m_0, and one may find a $\tilde{\tau}$ or even a $\tilde{e}$ LSP. The large value of $m_{1/2}$ also keeps the rate of $b \to s\gamma$ under control unless m_A is small. The chargino constraint is similar to that in panel (a), whereas the m_h constraint is irrelevant due to the large value of $m_{1/2}$. Finally, the GUT mass-squared positivity constraint now allows larger values of $|\mu| \lesssim 1000$ GeV.

It is also interesting to examine the m_0 - $m_{1/2}$ plane in the NUHM [23]. In Fig. 7a, there is a bulk region at $m_{1/2} \sim 50$ GeV to 350 GeV, $m_0 \sim 50$ GeV to 150 GeV. As in the CMSSM, the $\tilde{\tau}_1$ is the LSP in the bigger area at larger $m_{1/2}$, and there are light (turquoise) shaded strips close to these forbidden regions where coannihilation suppresses the relic density sufficiently to be cosmologically acceptable. Further away from these regions, the relic density is generally too high. However, for larger $m_{1/2}$ there is another suppression, discussed below, which makes the relic density too low. At small $m_{1/2}$ and m_0 the left handed sleptons, and also the sneutrinos, become lighter than the neutralino.

[2] This is similar to the focus-point region [18] in the CMSSM.

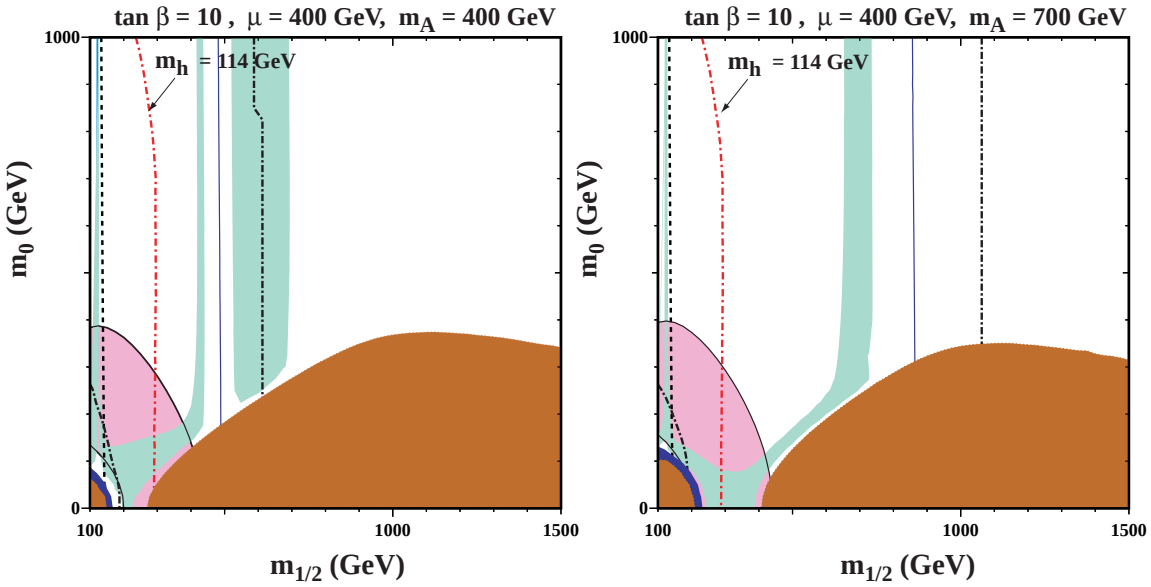

Figure 7: *Compilations of phenomenological constraints on the MSSM with NUHM in the* $(m_{1/2}, m_0)$ *plane for* $\tan\beta = 10$ *and (a)* $\mu = 400$ *GeV,* $m_A = 400$ *GeV, (b)* $\mu = 400$ *GeV,* $m_A = 700$ *GeV, again assuming* $A_0 = 0$*. The shading is consistent with previous figures. The (blue) solid line is the contour* $m_\chi = m_A/2$*, near which rapid direct-channel annihilation suppresses the relic density. The dark (black) dot-dashed lines indicates when one or another Higgs mass-squared becomes negative at the GUT scale: only intermediate values of* $m_{1/2}$ *are allowed.*

The darker (dark blue) shaded area is where a sneutrino is the LSP.

The near-vertical dark (black) dashed and light (red) dot-dashed lines in Fig. 7 are the LEP exclusion contours $m_{\chi^\pm} > 104$ GeV and $m_h > 114$ GeV respectively. As in the CMSSM case, they exclude low values of $m_{1/2}$, and hence rule out rapid relic annihilation via direct-channel h and Z^0 poles. The solid lines curved around small values of $m_{1/2}$ and m_0 bound the light (pink) shaded region favoured by a_μ and recent analyses of the e^+e^- data.

A striking feature in Fig. 7(a) when $m_{1/2} \sim 500$ GeV is a strip with low $\Omega_\chi h^2$, which has bands with acceptable relic density on either side. The low-$\Omega_\chi h^2$ strip is due to rapid annihilation via the direct-channel A, H poles which occur when $m_\chi = m_A/2 = 200$ GeV, indicated by the near-vertical solid (blue) line. The analogous rapid-annihilation strips occur in the CMSSM but at larger $\tan\beta$ as seen in Fig. 4. There, they are diagonal in the $(m_{1/2}, m_0)$ plane, reflecting a CMSSM link between m_0 and m_A that is absent in this implementation of the NUHM. The right-hand band in Fig. 7(a) with acceptable $\Omega_\chi h^2$ is broadened because the neutralino acquires significant Higgsino content, and the relic density is suppressed by the increased W^+W^- production. As $m_{1/2}$ increases, the neutralino becomes almost degenerate with the second lightest neutralino and the lighter chargino, and the $\chi - \chi' - \chi^\pm$ coannihilation processes eventually push $\Omega_\chi h^2 < 0.1$ when $m_{1/2} \gtrsim 700$ GeV.

The two dark (black) dash-dotted lines in Fig. 7(a) indicate where scalar squared

masses become negative at the input GUT scale for one of the Higgs multiplets. One of these GUT stability lines is near-vertical at $m_{1/2} \sim 600$ GeV, and the other is a curved line at $m_{1/2} \sim 150$ GeV, $m_0 \sim 200$ GeV.

Panel (b) of Fig. 7 is for $\mu = 400$ GeV and $m_A = 700$ GeV. We notice immediately that the heavy Higgs pole and the right-hand boundary of the GUT stability region move out to larger $m_{1/2} \sim 850, 1050$ GeV, respectively, as one would expect for larger m_A. At this value of m_A, the right side of the rapid annihilation ('funnel') strip has disappeared, due to enhanced chargino-neutralino coannihilation effects.

These two examples serve to demonstrate that the $(m_{1/2}, m_0)$ plane may look rather different in the CMSSM from its appearance in the CMSSM for the same value of $\tan\beta$. In particular, the locations of rapid-annihilation funnels and $\chi - \chi' - \chi^{\pm}$ coannihilation regions are quite model-dependent, and the GUT stability requirement may exclude large parts of the $(m_{1/2}, m_0)$ plane.

4.1 Detection

Because the LSP as dark matter is present locally, there are many avenues for pursuing dark matter detection. Direct detection techniques rely on an ample neutralino-nucleon scattering cross-section. The effective four-fermion lagrangian can be written as

$$\begin{aligned} \mathcal{L} &= \bar{\chi}\gamma^{\mu}\gamma^5\chi\bar{q}_i\gamma_{\mu}(\alpha_{1i} + \alpha_{2i}\gamma^5)q_i \\ &+ \alpha_{3i}\bar{\chi}\chi\bar{q}_i q_i + \alpha_{4i}\bar{\chi}\gamma^5\chi\bar{q}_i\gamma^5 q_i \\ &+ \alpha_{5i}\bar{\chi}\chi\bar{q}_i\gamma^5 q_i + \alpha_{6i}\bar{\chi}\gamma^5\chi\bar{q}_i q_i \end{aligned} \tag{15}$$

However, the terms involving $\alpha_{1i}, \alpha_{4i}, \alpha_{5i}$, and α_{6i} lead to velocity dependent elastic cross sections. The remaining terms are: the spin dependent coefficient, α_{2i} and the scalar coefficient α_{3i}. Contributions to α_{2i} are predominantly through light squark exchange. This is the dominant channel for binos. Scattering also occurs through Z exchange but this channel requires a strong Higgsino component. Contributions to α_{3i} are also dominated by light squark exchange but Higgs exchange is non-negligible in most cases.

Fig. 8 displays contours of the spin-independent cross section for the elastic scattering of the LSP χ on protons in the $m_{1/2}, m_0$ planes for (a) $\tan\beta = 10, \mu < 0$, (b) $\tan\beta = 10, \mu > 0$ [39]. The double dot-dashed (orange) lines are contours of the spin-independent cross section, and the contours $\sigma_{SI} = 10^{-9}$ pb in panel (a) and $\sigma_{SI} = 10^{-12}$ pb in panel (b) are indicated. The LEP lower limits on m_h and $m_{\chi^{\pm}}$, as well as the experimental measurement of $b \to s\gamma$ for $\mu < 0$, tend to bound the cross sections from above, as discussed in more detail below. Generally speaking, the spin-independent cross section is relatively large in the 'bulk' region, but falls off in the coannihilation 'tail'. Also, we note also that there is a strong cancellation in the spin-independent cross section when $\mu < 0$ [40, 41], as seen along strips in panel (a) of Fig. 8 where $m_{1/2} \sim 500$ GeV. In the cancellation region, the cross section drops lower than 10^{-14} pb. All these possibilities for suppressed spin-independent cross sections are disfavoured by the data on $g_{\mu} - 2$, which favour values of $m_{1/2}$ and m_0 that are not very large, as well as $\mu > 0$, as seen in panel (b) of Fig. 8. Thus $g_{\mu} - 2$ tends to provide a lower bound on the spin-independent cross section.

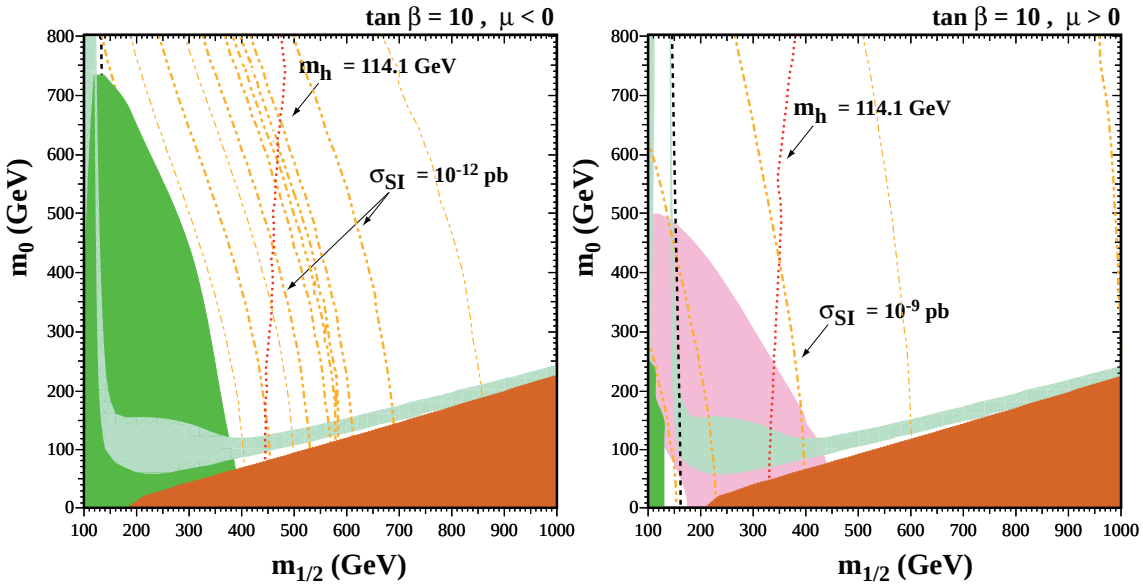

Figure 8: *Spin-independent cross sections in the* $(m_{1/2}, m_0)$ *planes for (a)* $\tan\beta = 10, \mu < 0$*, (b)* $\tan\beta = 10, \mu > 0$*. The double dot-dashed (orange) curves are contours of the spin-independent cross section, differing by factors of 10 (bolder) and interpolating factors of 3 (finer - when shown). For example, in (b), the curves to the right of the one marked* 10^{-9} *pb correspond to* 3×10^{-10} *pb and* 10^{-10} *pb.*

Fig. 9(a) illustrates the effect on the cross sections of each of the principal phenomenological constraints, for the particular case $\tan\beta = 10$ $\mu > 0$. The solid (blue) lines mark the bounds on the cross sections allowed by the relic-density constraint $0.1 < \Omega_\chi h^2 < 0.3$ alone. For any given value of $m_{1/2}$, only a restricted range of m_0 is allowed. Therefore, only a limited range of m_0, and hence only a limited range for the cross section, is allowed for any given value of m_χ. The thicknesses of the allowed regions are due in part to the assumed uncertainties in the nuclear inputs. These have been discussed at length in [41, 40]. On the other hand, a broad range of m_χ is allowed, when one takes into account the coannihilation 'tail' region at each $\tan\beta$ and the rapid-annihilation 'funnel' regions for $\tan\beta = 35, 50$. The dashed (black) line displays the range allowed by the $b \to s\gamma$ constraint alone. In this case, a broader range of m_0 and hence the spin-independent cross section is possible for any given value of m_χ. The impact of the constraint due to m_h is shown by the dot-dashed (green) line. Comparing with the previous constraints, we see that a region at low m_χ is excluded by m_h, strengthening significantly the previous *upper* limit on the spin-independent cross section. Finally, the dotted (red) lines in Fig. 9 show the impact of the $g_\mu - 2$ constraint. This imposes an upper bound on $m_{1/2}$ and hence m_χ, and correspondingly a *lower* limit on the spin-independent cross section.

This analysis is extended in panel (b) of Fig. 9 to all the values $8 < \tan\beta \leq 55$ and we find overall that [39]

$$2 \times 10^{-10}\ \text{pb} \lesssim \quad \sigma_{SI} \quad \lesssim 6 \times 10^{-8}\ \text{pb}, \tag{16}$$

$$2 \times 10^{-7}\ \text{pb} \lesssim \quad \sigma_{SD} \quad \lesssim 10^{-5}\ \text{pb}, \tag{17}$$

for $\mu > 0$. (σ_{SD} is the spin-dependent cross-section not shown in the figures presented

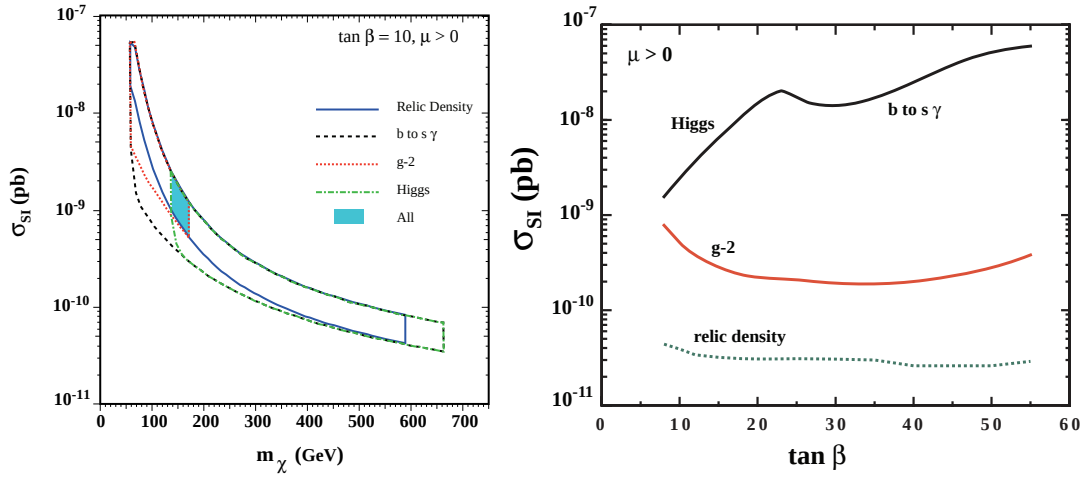

Figure 9: *Allowed ranges of the cross sections for* $\tan\beta = 10$ *(a)* $\mu > 0$ *for spin-independent elastic scattering. The solid (blue) lines indicate the relic density constraint, the dashed (black) lines the* $b \to s\gamma$ *constraint, the dot-dashed (green) lines the* m_h *constraint, and the dotted (red) lines the* $g_\mu - 2$ *constraint. The shaded (pale blue) region is allowed by all the constraints. (b) The allowed ranges of the spin-independent cross section for* $\mu > 0$*. The darker solid (black) lines show the upper limits on the cross sections obtained from* m_h *and* $b \to s\gamma$*, and (where applicable) the lighter solid (red) lines show the lower limits suggested by* $g_\mu - 2$ *and the dotted (green) lines the lower limits from the relic density.*

here.) As we see in panel (b) of Fig. 9, m_h provides the most important upper limit on the cross sections for $\tan\beta < 23$, and $b \to s\gamma$ for larger $\tan\beta$, with $g_\mu - 2$ always providing a more stringent lower limit than the relic-density constraint. The relic density constraint shown is evaluated at the endpoint of the coannihilation region. At large $\tan\beta$, the Higgs funnels or the focus-point regions have not been considered, as their locations are very sensitive to input parameters and calculational details [42].

The results from a CMSSM and MSSM analysis [40, 41] for $\tan\beta = 3$ and 10 are compared with the most recent CDMS [43] and Edelweiss [44] bounds in Fig. 10. These results have nearly entirely excluded the region purported by the DAMA [45] experiment. The CMSSM prediction [40] is shown by the dark shaded region, while the NUHM case [41] is shown by the larger lighter shaded region.

I conclude by showing the prospects for direct detection for the benchmark points discussed above[46]. Fig. 11 shows rates for the elastic spin-independent scattering of supersymmetric relics, including the projected sensitivities for CDMS II [47] and CRESST [48] (solid) and GENIUS [49] (dashed). Also shown are the cross sections calculated in the proposed benchmark scenarios discussed in the previous section, which are considerably below the DAMA [45] range ($10^{-5} - 10^{-6}$ pb). Indirect searches for supersymmetric dark matter via the products of annihilations in the galactic halo or inside the Sun also have prospects in some of the benchmark scenarios [46].

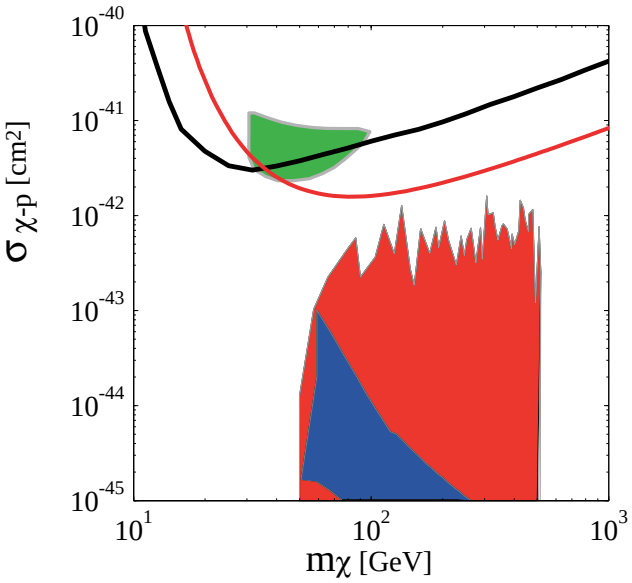

Figure 10: *Limits from the CDMS [43] and Edelweiss [44] experiments on the neutralino-proton elastic scattering cross section as a function of the neutralino mass. The Edelweiss limit is stronger at higher m_χ. These results nearly exclude the shaded region observed by DAMA [45]. The theoretical predictions lie at lower values of the cross section.*

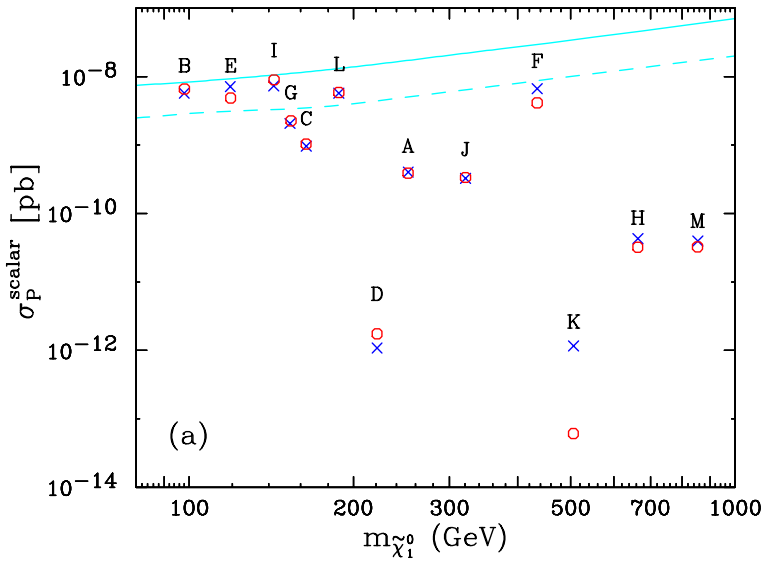

Figure 11: *Elastic spin-independent scattering of supersymmetric relics on protons calculated in benchmark scenarios[46], compared with the projected sensitivities for CDMS II [47] and CRESST [48] (solid) and GENIUS [49] (dashed). The predictions of our code (blue crosses) and* `Neutdriver` *[50] (red circles) for neutralino-nucleon scattering are compared. The labels correspond to the benchmark points as shown in Fig. 1.*

Acknowledgments

I would like to thank J. Ellis, T. Falk, A. Ferstl, G. Ganis, Y. Santoso, and M. Srednicki for enjoyable collaborations from which this work is culled. This work was supported in part by DOE grant DE-FG02-94ER40823 at Minnesota.

References

[1] J. Ellis, J.S. Hagelin, D.V. Nanopoulos, K.A. Olive, and M. Srednicki, *Nucl. Phys.* **B238**, 453 (1984);
see also H. Goldberg, *Phys. Rev. Lett.* **50**, 1419 (1983).

[2] J. Rich, M. Spiro, and J. Lloyd-Owen, *Phys.Rep.* **151**, 239 (1987);
P.F. Smith, *Contemp.Phys.* **29**, 159 (1998);
T.K. Hemmick et al., *Phys.Rev.* **D41**, 2074 (1990). T. Yanagata, Y. Takamori, and H. Utsunomiya, *Phys.Rev.* **D47**, 1231 (1993).

[3] L.E. Ibanez, *Phys. Lett.* **137B**, 160 (1984);
J. Hagelin, G.L. Kane, and S. Raby, *Nucl., Phys.* **B241**, 638 (1984).

[4] T. Falk, K. A. Olive, and M. Srednicki, Phys. Lett. B **339**, 248 (1994) [arXiv:hep-ph/9409270].

[5] S. Ahlen, et. al., *Phys. Lett.* **B195**, 603 (1987);
D.D. Caldwell, et. al., *Phys. Rev. Lett.* **61**, 510 (1988);
M. Beck et al., *Phys. Lett.* **B336** 141 (1994).

[6] see e.g. K.A. Olive and M. Srednicki, *Phys. Lett.* **205B**, 553 (1988);
N. Sato et al. *Phys.Rev.* **D44**, 2220 (1991).

[7] J. R. Ellis, T. Falk, K. A. Olive, and M. Schmitt, Phys. Lett. B **388**, 97 (1996) [arXiv:hep-ph/9607292];
The LEP Collaborations, the LEP Electroweak Working Group, and the SLD Heavy Flavour and Electroweak Groups, CERN-EP-2000-016.

[8] R. Watkins, M. Srednicki, and K.A. Olive, *Nucl. Phys.* **B310**, 693 (1988).

[9] P. Hut, *Phys. Lett.* **69B**, 85 (1977);
B.W. Lee and S. Weinberg, *Phys. Rev. Lett.* **39**, 165 (1977).

[10] G. Steigman, K. A. Olive, and D. N. Schramm, *Phys. Rev. Lett.* **43**, 239 (1979);
K. A. Olive, D. N. Schramm and G. Steigman, *Nucl. Phys. B* **180**, 497 (1981).

[11] K. Griest and D. Seckel, *Phys.Rev.* **D43**, 3191 (1991).

[12] A. Melchiorri and J. Silk, Phys. Rev. D **66** (2002) 041301 [arXiv:astro-ph/0203200].

[13] J. R. Ellis, T. Falk, and K. A. Olive, Phys. Lett. B **444**, 367 (1998) [arXiv:hep-ph/9810360];
J. R. Ellis, T. Falk, K. A. Olive, and M. Srednicki, Astropart. Phys. **13**, 181 (2000) [Erratum-ibid. **15**, 413 (2001)] [arXiv:hep-ph/9905481].

[14] M. E. Gómez, G. Lazarides, and C. Pallis, Phys. Rev. **D61**, 123512 (2000) [hep-ph/9907261]; Phys. Lett. **B487**, 313 (2000) [hep-ph/0004028]; Nucl. Phys. B **638** (2002) 165 [arXiv:hep-ph/0203131];
R. Arnowitt, B. Dutta, and Y. Santoso, hep-ph/0102181.

[15] C. Boehm, A. Djouadi, and M. Drees, Phys. Rev. D **62**, 035012 (2000) [arXiv:hep-ph/9911496];
J. Ellis, K.A. Olive and Y. Santoso, arXiv:hep-ph/0112113.

[16] M. Drees and M. M. Nojiri, *Phys. Rev. D* **47**, 376 (1993);
H. Baer and M. Brhlik, *Phys. Rev. D* **53**, 597 (1996) ;and *Phys. Rev. D* **57** 567 (1998);
H. Baer, M. Brhlik, M. A. Diaz, J. Ferrandis, P. Mercadante, P. Quintana and X. Tata, *Phys. Rev. D* **63**, 015007 (2001);
A. B. Lahanas, D. V. Nanopoulos and V. C. Spanos, *Mod. Phys. Lett. A* **16** 1229 (2001).

[17] J. Ellis, T. Falk, G. Ganis, K. A. Olive, and M. Srednicki, hep-ph/0102098.

[18] J. L. Feng, K. T. Matchev, and F. Wilczek, Phys. Lett. B **482**, 388 (2000) [hep-ph/0004043].

[19] M. Battaglia et al., *Eur. Phys. J. C* **22** 535 (2001).

[20] S. Heinemeyer, W. Hollik, and G. Weiglein, Comput. Phys. Commun. **124** (2000) 76 [arXiv:hep-ph/9812320];
S. Heinemeyer, W. Hollik, and G. Weiglein, Eur. Phys. J. C **9** (1999) 343 [arXiv:hep-ph/9812472].

[21] J. R. Ellis, T. Falk, G. Ganis, and K. A. Olive, Phys. Rev. D **62**, 075010 (2000) [arXiv:hep-ph/0004169].

[22] J. R. Ellis, K. A. Olive, and Y. Santoso, New J. Phys. **4** (2002) 32 [arXiv:hep-ph/0202110].

[23] J. Ellis, K. Olive, and Y. Santoso, Phys. Lett. B **539**, 107 (2002);
J. Ellis, T. Falk, K. A. Olive and Y. Santoso, arXiv:hep-ph/0210205.

[24] Joint LEP 2 Supersymmetry Working Group, *Combined LEP Chargino Results, up to 208 GeV*,
`http://lepsusy.web.cern.ch/lepsusy/www/inos_moriond01/charginos_pub.html`.

[25] Joint LEP 2 Supersymmetry Working Group, *Combined LEP Selectron/Smuon/Stau Results, 183-208 GeV*,
`http://alephwww.cern.ch/~ganis/SUSYWG/SLEP/sleptons_2k01.html`.

[26] LEP Higgs Working Group for Higgs boson searches, OPAL Collaboration, ALEPH Collaboration, DELPHI Collaboration and L3 Collaboration, *Search for the Standard Model Higgs Boson at LEP*, ALEPH-2001-066, DELPHI-2001-113, CERN-L3-NOTE-2699, OPAL-PN-479, LHWG-NOTE-2001-03, CERN-EP/2001-055, arXiv:hep-ex/0107029; *Searches for the neutral Higgs bosons of the MSSM: Preliminary combined results using LEP data collected at energies up to 209 GeV*, LHWG-NOTE-2001-04, ALEPH-2001-057, DELPHI-2001-114, L3-NOTE-2700, OPAL-TN-699, arXiv:hep-ex/0107030.

[27] M.S. Alam et al., [CLEO Collaboration], *Phys. Rev. Lett.* **74**, 2885 (1995);
as updated in S. Ahmed et al., CLEO CONF 99-10; BELLE Collaboration, BELLE-CONF-0003, contribution to the 30th International conference on High-Energy Physics, Osaka, 2000;
See also K. Abe *et al.*, [Belle Collaboration], [arXiv:hep-ex/0107065];
L. Lista [BaBar Collaboration], [arXiv:hep-ex/0110010];
C. Degrassi, P. Gambino, and G. F. Giudice, *JHEP* **0012**, 009 (2000);
M. Carena, D. Garcia, U. Nierste, and C. E. Wagner, *Phys. Lett. B* **499**, 141 (2001);
P. Gambino and M. Misiak, Nucl. Phys. B **611** (2001) 338;
D. A. Demir and K. A. Olive, Phys. Rev. D **65**, 034007 (2002).

[28] G. W. Bennett *et al.* [Muon g-2 Collaboration], Phys. Rev. Lett. **89** (2002) 101804 [Erratum-ibid. **89** (2002) 129903] [arXiv:hep-ex/0208001].

[29] M. Davier, S. Eidelman, A. Hocker, and Z. Zhang, arXiv:hep-ph/0208177; see also K. Hagiwara, A. D. Martin, D. Nomura, and T. Teubner, arXiv:hep-ph/0209187; F. Jegerlehner (unpublished, as reported in M. Krawczyk, arXiv:hep-ph/0208076.

[30] A. B. Lahanas, D. V. Nanopoulos, and V. C. Spanos, Phys. Lett. B **518** (2001) 94 [arXiv:hep-ph/0107151];
V. Barger and C. Kao, Phys. Lett. B **518**, 117 (2001) [arXiv:hep-ph/0106189];
L. Roszkowski, R. Ruiz de Austri, and T. Nihei, JHEP **0108**, 024 (2001) [arXiv:hep-ph/0106334];
A. Djouadi, M. Drees, and J. L. Kneur, JHEP **0108**, 055 (2001) [arXiv:hep-ph/0107316];
H. Baer, C. Balazs and A. Belyaev, JHEP **0203**, 042 (2002) [arXiv:hep-ph/0202076].

[31] V. Berezinsky, A. Bottino, J. R. Ellis, N. Fornengo, G. Mignola, and S. Scopel, Astropart. Phys. **5**, 1 (1996) [arXiv:hep-ph/9508249];
P. Nath and R. Arnowitt, Phys. Rev. D **56**, 2820 (1997) [arXiv:hep-ph/9701301];
M. Drees, M. M. Nojiri, D. P. Roy, and Y. Yamada, Phys. Rev. D **56**, 276 (1997) [Erratum-ibid. D **64**, 039901 (1997)] [arXiv:hep-ph/9701219];
M. Drees, Y. G. Kim, M. M. Nojiri, D. Toya, K. Hasuko, and T. Kobayashi, Phys. Rev. D **63**, 035008 (2001) [arXiv:hep-ph/0007202].

[32] J. R. Ellis, T. Falk, G. Ganis, K. A. Olive, and M. Schmitt, Phys. Rev. D **58** (1998) 095002 [arXiv:hep-ph/9801445].

[33] V. D. Barger, M. S. Berger, and P. Ohmann, Phys. Rev. D **49** (1994) 4908 [arXiv:hep-ph/9311269].

[34] W. de Boer, R. Ehret, and D. I. Kazakov, Z. Phys. C **67** (1995) 647 [arXiv:hep-ph/9405342].

[35] M. Carena, J. R. Ellis, A. Pilaftsis, and C. E. Wagner, Nucl. Phys. B **625** (2002) 345 [arXiv:hep-ph/0111245].

[36] L. E. Ibanez, C. Lopez, and C. Munoz, Nucl. Phys. B **256** (1985) 218.

[37] S. P. Martin and M. T. Vaughn, Phys. Rev. D **50** (1994) 2282 [arXiv:hep-ph/9311340].

[38] T. Falk, K. A. Olive, L. Roszkowski, and M. Srednicki, Phys. Lett. B **367** (1996) 183 [arXiv:hep-ph/9510308];
A. Riotto and E. Roulet, Phys. Lett. B **377** (1996) 60 [arXiv:hep-ph/9512401];
A. Kusenko, P. Langacker and G. Segre, Phys. Rev. D **54** (1996) 5824 [arXiv:hep-ph/9602414];
T. Falk, K. A. Olive, L. Roszkowski, A. Singh, and M. Srednicki, Phys. Lett. B **396** (1997) 50 [arXiv:hep-ph/9611325].

[39] J. R. Ellis, A. Ferstl, and K. A. Olive, Phys. Lett. B **532**, 318 (2002).

[40] J. R. Ellis, A. Ferstl, and K. A. Olive, Phys. Lett. B **481**, 304 (2000).

[41] J. R. Ellis, A. Ferstl, and K. A. Olive, Phys. Rev. D **63**, 065016 (2001).

[42] J. R. Ellis and K. A. Olive, Phys. Lett. B **514**, 114 (2001) [arXiv:hep-ph/0105004].

[43] D. Abrams *et al.* [CDMS Collaboration], arXiv:astro-ph/0203500.

[44] R. Jakob, arXiv:hep-ph/0206271.

[45] DAMA Collaboration, R. Bernabei *et al.*, *Phys. Lett. B* **436** (1998) 379.

[46] J. Ellis, J. L. Feng, A. Ferstl, K. T. Matchev, and K. A. Olive, Eur. Phys. J. C **24**, 311 (2002) [arXiv:astro-ph/0110225].

[47] CDMS Collaboration, R. W. Schnee *et al.*, *Phys. Rept.* **307**, 283 (1998).

[48] CRESST Collaboration, M. Bravin *et al.*, *Astropart. Phys.* **12**, 107 (1999).

[49] H. V. Klapdor-Kleingrothaus, arXiv:hep-ph/0104028.

[50] G. Jungman, M. Kamionkowski, and K. Griest, *Phys. Rept.* **267**, 195 (1996); `http://t8web.lanl.gov/people/jungman/neut-package.html`.